Punching shear analysis of reinforced high-strength concrete slabs

H. MARZOUK AND A. HUSSEIN

Faculty of Engineering and Applied Science, Memorial University of Newfoundland, St. John's, Nfld., Canada A1B 3X5

Received November 16, 1990

Revised manuscript accepted April 25, 1991

An experimental investigation was conducted at the structural laboratory at Memorial University of Newfoundland to examine the behaviour of high-strength concrete two-way slabs. It was evident that a new mechanical model is required to predict the punching shear capacity of such slabs. The experimental results of the tested slabs with regard to deformations, strains, ultimate capacity, and modes of failure were examined. Based on the test results, a mechanical model was adopted and developed for high-strength concrete slab applications. The formulation takes into account the actual behaviour of the high-strength concrete and steel. The proposed model gives a fairly good agreement between the predicted and experimental punching loads.

Key words: deflections, deformations, failure mechanisms, flat concrete plates, high-strength concrete, loads (forces), mechanical model, punching shear, reinforced concrete.

À la suite d'une étude expérimentale réalisée au laboratoire des structures du Memorial University of Newfoundland afin d'examiner le comportement de dalles de béton à deux voies à haute résistance, les chercheurs ont constaté la nécessité d'un nouveau modèle mécanique afin de prédire la contrainte de poinçonnement de ces dalles. Les résultats expérimentaux des essais relatifs à la déformation, à l'effort, à la capacité ultime et aux modes de défaillance ont été examinés. Compte tenu de ces résultats, un modèle mécanique a été adopté et élaboré pour les dalles de béton à haute résistance. La formule tient compte du comportement actuel du béton à haute résistance et de l'acier. Le modèle proposé permet d'obtenir une assez bonne concordance entre les charges de poinçonnement prévues et celles mesurées en laboratoire.

Mots clés : flèches, déformations, mécanismes de défaillance, plaques de béton plates, béton à haute résistance, charges (forces), modèle mécanique, contrainte de poinçonnement, béton armé.

[Traduit par la rédaction]

Can. J. Civ. Eng. **18**, 954–963 (1991)

Introduction

Research on punching shear has yielded a number of methods by which the ultimate shearing strength of slabs can be predicted. In general, the various suggested approaches can be described as either the results of an empirical study, in which a statistical analysis of the available test results is used to establish a relationship between the load or stress at failure and the parameters of the slab, or the result of a rational study, in which the strength of the slab materials and the mechanism of failure are idealized and described mathematically.

The ACI 318 (American Concrete Institute 1989) and CSA (CAN3-A23.3-M84) (Canadian Standards Association 1984) codes are based mainly on Moe's work (1961), while the BS 8110 (British Standard Institution 1985) code is based on Regan's work (1974). These present building code specifications for the shear strength of reinforced concrete slabs are based on the test results of slabs made with relatively low compressive strengths, varying mostly from 14 to 40 MPa. Test results revealed that the present North American codes overestimate the influence of the concrete strength, as a factor, on the ultimate capacity of two-way slabs. Hence, it is necessary to develop a rational model to predict the ultimate shear strength of two-way slabs made with high-strength concrete.

The experimental program carried out on 17 concrete slabs has provided the basis for the proposed model. The test results revealed that the Kinnunen and Nylander rational model (1960) still provides the best account of the punching behaviour of concrete slabs. A modification and adaptation for the use of this model for high-strength concrete slabs is presented.

NOTE: Written discussion of this paper is welcomed and will be received by the Editor until April 30, 1992 (address inside front cover).

Summary of experimental investigation

The dimensions and reinforcement details of the tested slabs are given in Table 1. Figure 1 depicts a typical test specimen and the arrangement of concrete and steel gauges. A typical slab during testing is shown in Fig. 2.

The load–deflection curves of the tested slabs under concentrated central load can be used to classify the type of slab failure. Failure modes can be classified into three categories: pure flexural failure, pure punching failure, and ductile shear failure. Pure flexural failure takes place in slabs where most of the reinforcement yields before punching occurs and, consequently, the slab exhibits large deflections prior to failure. Pure shear failure occurs when the slab shows small deflections, with yielding of the tension steel being very localized at the column head. The third type of failure, ductile shear failure, is a transition between the cases of pure punching and pure flexure failures. In general, the load–deflection curve for the slabs failing in punching can be represented by two straight lines with different slopes, as shown in Fig. 3. The first line has a slope corresponding to the stiffness of the uncracked slab and applies up to the initial cracking load. The second line extends up to the load that caused the first yielding in the tension reinforcement. The slope of this line represents the stiffness of the cracked slab, μ. Ductility is quantified in terms of the ratio of the deflection at the ultimate load to the deflection at the first yielding of flexural reinforcement. The energy absorption is defined as the area under the load–deflection curve. The ductility decreased as the reinforcement was increased. Ductility is slightly increased with the increase in concrete strength. Also, increasing the column size increased the ductility. The energy absorption of the slabs is decreased as the reinforcement increased. Slabs failing in flexure showed a higher energy absorption capacity than those failing in shear.

Printed in Canada / Imprimé au Canada

TABLE 1. Details of test specimens

Slab series	Slab designation*	Compressive strength f'_c (MPa)	Slab thickness (mm)	Average depth (mm)	Column size (mm)	Reinforcement details†	Reinforcement ratio ρ (%)
I	NS1	42	120	95	150	21 – M 10	1.474
	HS1	67	120	95	150	7 – M 10	0.491
	HS2	70	120	95	150	12 – M 10	0.842
	HS7	74	120	95	150	17 – M 10	1.193
	HS3	69	120	95	150	21 – M 10	1.474
	HS4	66	120	90	150	16 – M 15	2.370
II	NS2	30	150	120	150	17 – M 10	0.944
	HS5	68	150	125	150	12 – M 10	0.640
	HS6	70	150	120	150	17 – M 10	0.944
	HS8	69	150	120	150	10 – M 15	1.111
	HS9	74	150	120	150	15 – M 15	1.611
	HS10	80	150	120	150	21 – M 15	2.333
III	HS11	70	90	70	150	10 – M 10	0.952
	HS12	75	90	70	150	16 – M 10	1.524
	HS13	68	90	70	150	21 – M 10	2.000
IV	HS14	72	120	95	220	21 – M 10	1.474
	HS15	71	120	95	300	21 – M 10	1.474

*NS, normal-strength slabs; HS, high-strength slabs.
†Data given are for lower reinforcement; for upper reinforcement, 5 – M 10 is used for all specimens.

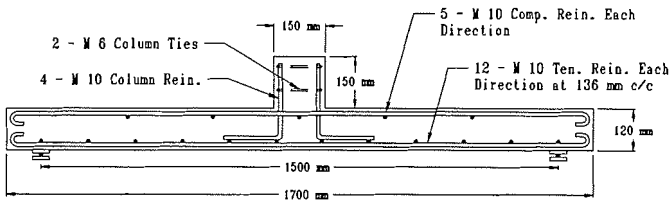

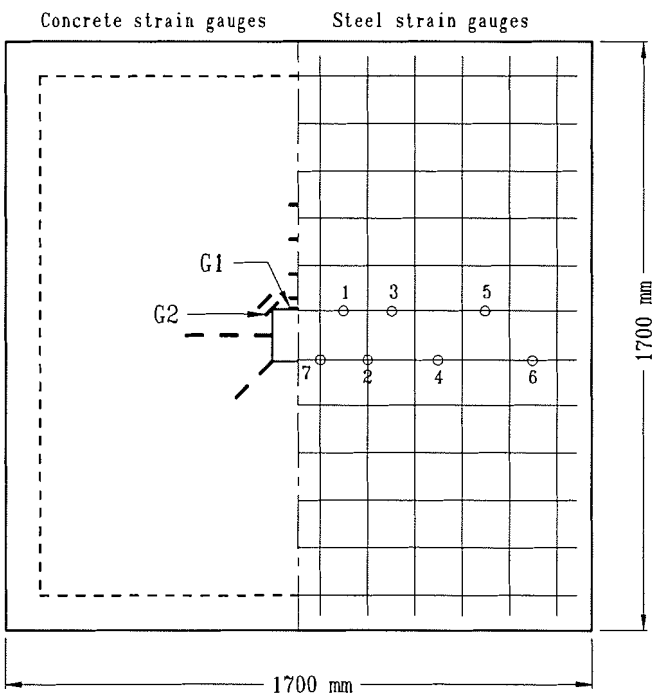

FIG. 1. Details of a typical test specimen and strain gauge locations.

The observed values of the angle of rotation, at failure, of the slab portion outside the shear crack are presented in Table 2. The slab rotation decreased with increasing reinforcement ratio and concrete strength.

For all the tested slabs, measurements were made to determine the concrete and steel strain distributions. A typical arrangement of the concrete and steel gauges is shown in Fig. 1. The concrete radial strains were high at the column face, but they decreased rapidly as the radius increased. In some cases, prior to failure, the radial strains at the column face started to decrease. The strains in the tangential direction have smaller gradients than those in the radial direction; and with good approximation these tangential strains can be assumed inversely proportional to the radius, as proposed by Kinnunen and Nylander (1960). Also, a concentration of stress was evident at the corners of the column stub. Neither the concrete strains in the tangential direction nor those in the radial direction reached a limiting value of 0.0035 for any of the tested slabs. The maximum concrete strains, near failure, are also given in Table 2.

The highest steel strains, and consequently the initial yielding, occurred below the stub column. These recorded steel strains are also given in Table 2. In all the tested slabs, the tension reinforcement yielded before punching took place. The degree to which yielding spread in the reinforcement varied with the reinforcement ratio. At high reinforcement levels, the yield of tension reinforcement occurred at high loads and was localized at the column stub. For lightly reinforced slabs, yielding initiated at the column stub and gradually progressed throughout the whole tension reinforcement. The observed values of the radius of yield, r_y, which normally determine the extent of yielding of reinforcement in the slab, are given in Table 2.

The initial flexural cracks recorded for the test slabs were first formed tangentially under the edge of the column stub,

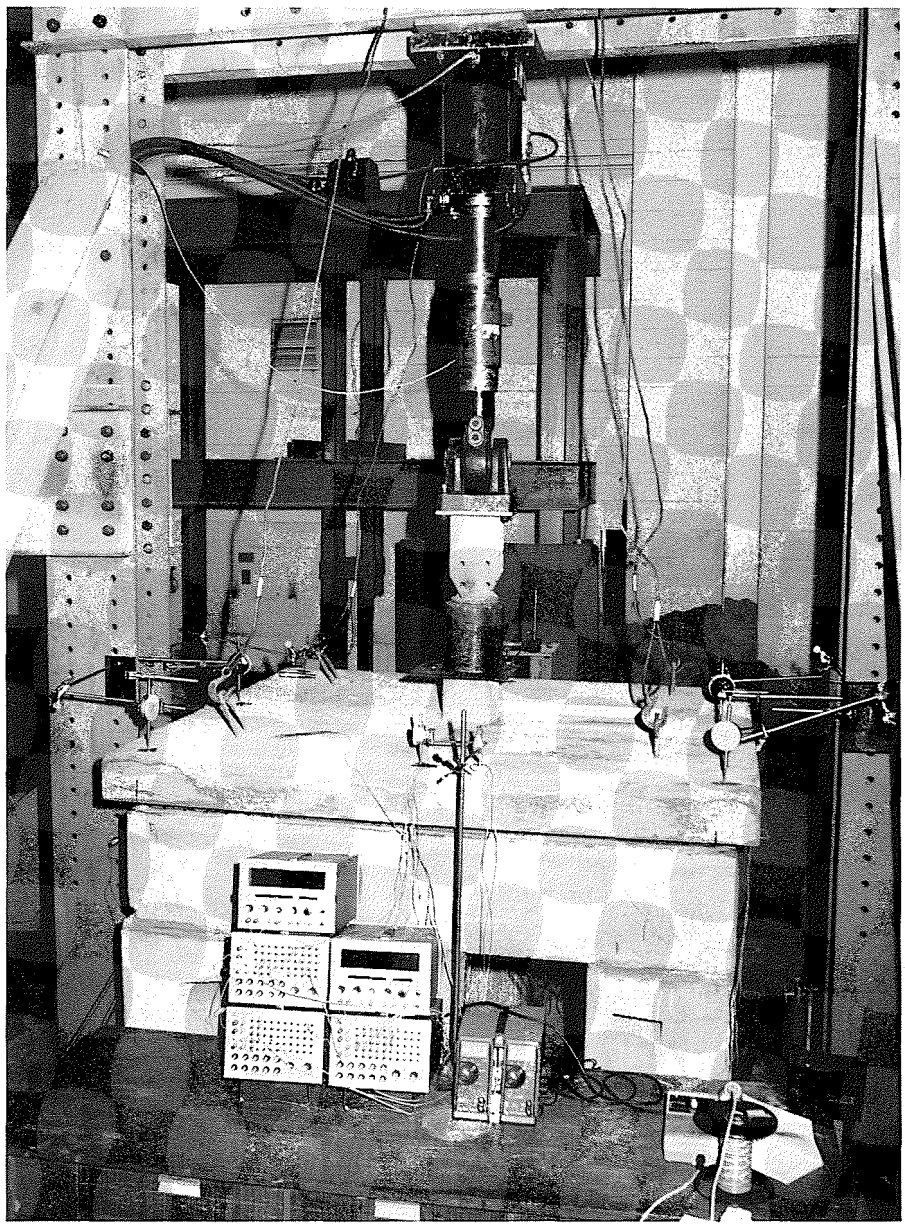

FIG. 2. Test setup.

followed by radial cracking extending from the column. The first radial cracks were much more pronounced along lines parallel to the reinforcement crossing through the column stub. As the load was increased, the tangential cracks were then extended outside the circumference of the stub column. It is worth mentioning here that these tangential cracks were limited to the column vicinity. The slabs failed with the final shear crack coinciding with, or located outside, these cracks. Final failure developed by the column punching through the slab, as shown in Fig. 4.

The punching shear surface on the tension face occurred at a distance of $1.2-1.6$ times the slab depth, d, from the column face for most of the test slabs. The failure surface of few of the test specimens were carefully removed and examined. The observed angles of failure surface varied considerably. For normal-strength concrete slabs, this angle was found to be between 26° and 30°, in agreement with Regan and Braestrup's reported data (1985), while for high-strength concrete slabs the observed angle of failure surface varied between 32° and 38°. A typical failure surface of high-strength concrete slab is shown in Fig. 5.

As expected, the ultimate punching shear load increased as the reinforcement ratio was increased. Also, increasing the compressive strength increased the ultimate punching load, but at a rate less than the square root of the slab compressive strength. The ultimate recorded test loads are also given in Table 2.

Punching failure mechanism

The slab is divided into rigid radial segments, each bounded by two radial crack lines, a part of the initial circumferential crack and the slab boundary, as illustrated in Fig. 6. The radial segment rotates around a centre of rotation (C.R.) located at the face of the column and on the level of the neutral axis, as proposed by other researchers. This idealized model allows the deformation of the part of the slab that is on the top of the column

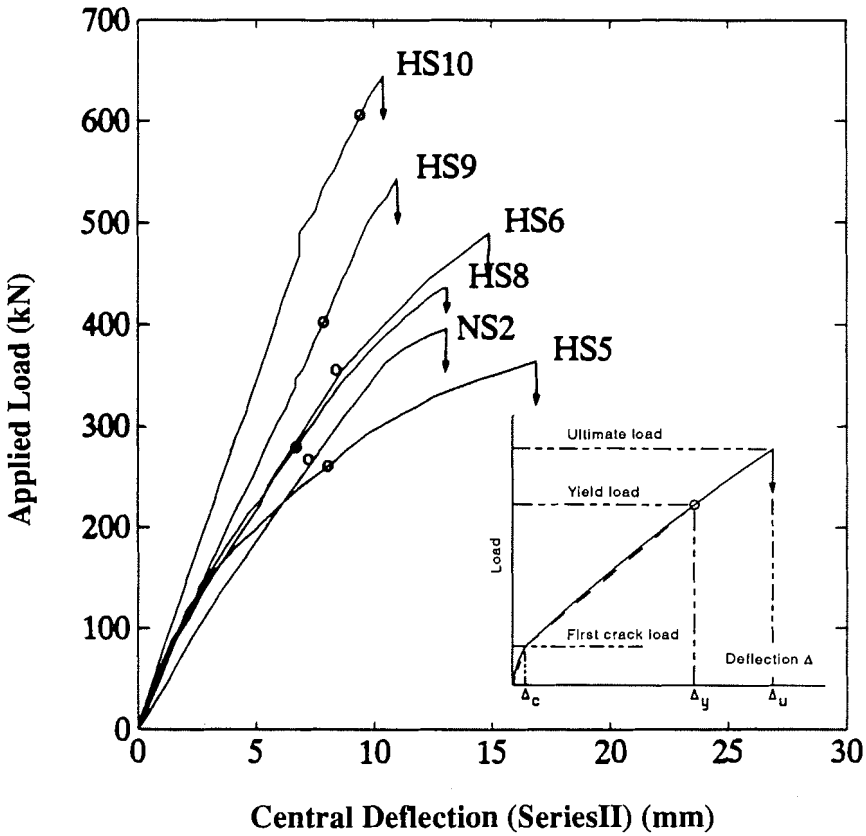

FIG. 3. Applied load versus central deflection (series II).

TABLE 2. Deformation characteristics of test slabs

Slab	Ultimate recorded load P_u (kN)	Ultimate steel strains* ε_{su} ($\times 10^{-3}$)	Ultimate concrete strain: Radial mid ε_{cr} ($\times 10^{-3}$)	Ultimate concrete strain: Tangential mid† ε_{ct} ($\times 10^{-3}$)	Ultimate concrete strain: Tangential corner‡ ε_c ($\times 10^{-3}$)	Ultimate rotation ψ ($\times 10^{-3}$ rad)	Radius of yield r_y (mm)	Mode of failure§
NS1	320	3.13	—	2.24	—	11.8	304	P
HS1	178	13.90	—	—	—	—	—	F
HS2	249	3.10	1.17	—	—	18.4	512	D
HS7	356	3.79	—	2.09	—	15.5	381	D
HS3	356	2.92	1.70	—	—	12.4	252	P
HS4	418	3.09	2.90	—	—	12.4	213	D
NS2	400	—	—	—	—	11.1	—	P
HS5	365	3.56	1.29	—	—	13.6	—	D
HS6	489	3.22	—	2.40	2.95	12.2	—	D
HS8	436	4.15	—	2.36	2.92	12.3	452	D
HS9	543	2.96	—	2.04	2.82	9.7	344	P
HS10	645	2.54	—	1.97	1.49	11.1	—	P
HS11	196	6.84	—	1.63	1.70	—	658	F
HS12	258	3.66	—	1.83	2.36	21.2	371	D
HS13	267	3.70	—	2.33	2.78	13.9	362	P
HS14	498	3.35	—	1.72	2.89	18.6	—	D
HS15	560	4.69	—	1.71	2.02	21.6	—	D

*Around the column periphery.
†Gauge G1, Fig. 1.
‡Gauge G2, Fig. 1.
§F = flexure failure; D = ductile punching failure; P = punching failure.

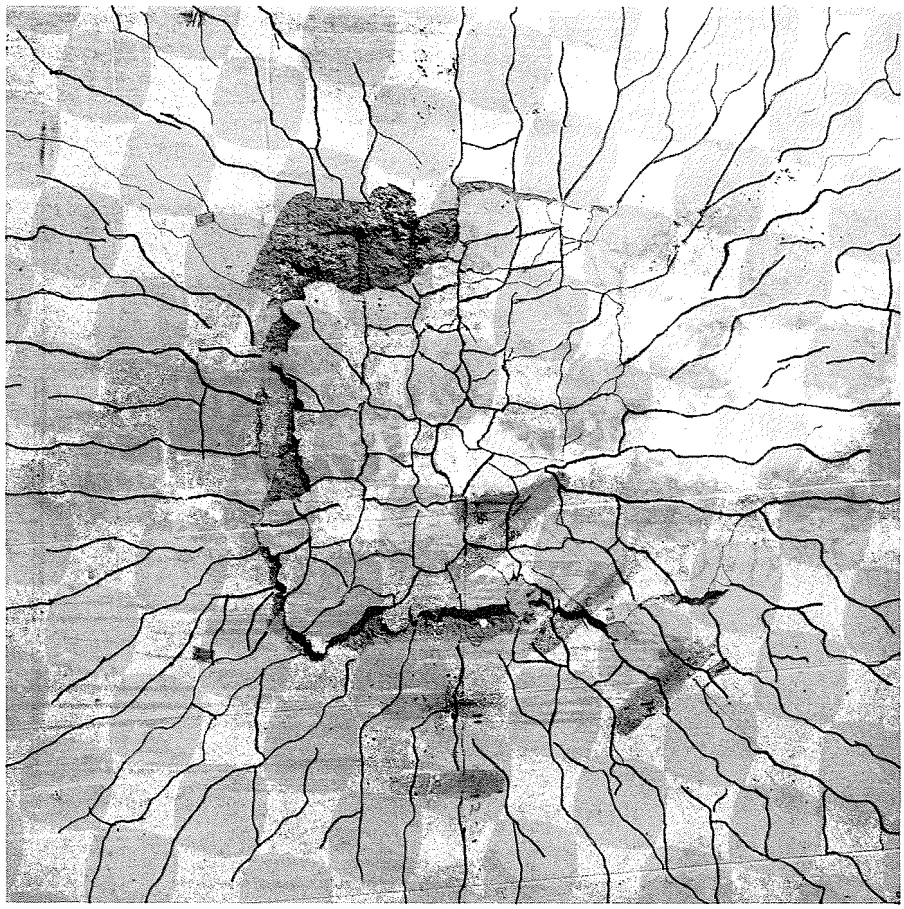

FIG. 4. Crack pattern at failure for a typical test slab.

and bounded by the shear crack. Thus, the dowel forces can be directly calculated from the model equilibrium. In previous models like the Kinnunen and Nylander's model (1960), this portion of the slab was considered to remain undeformed, in contradiction to the test results; and the dowel forces had an established fixed value of 30% of the ultimate load.

The part of the slab between two radial cracks is assumed to rotate as a rigid body between the slab edge and the column perimeter. On the basis of this assumption, the concrete and steel strains can be calculated as a function of the tangential curvature of the slab, as shown in Fig. 7. Hence, the tangential concrete strain, ε_{ct}, and the steel strain, ε_s, at a distance r from the centre of the slab can be calculated from the following expressions:

$$[1] \quad \varepsilon_{ct} = \psi \frac{x}{r}$$

and

$$[2] \quad \varepsilon_s = \psi \frac{d - x}{r}$$

The angle of the shear crack is hard to determine experimentally. However, the angle of inclination of the failure surface can be measured, as mentioned in the previous section. The assumed relation between the average angle of failure surface and the inclination of the shear crack is illustrated in Fig. 8. Hence, the punching radius, r_w, is equal to

$$[3] \quad r_w = r_0 + d \cot 30°$$

Stress–strain relationships

The stress–strain curve for the reinforcement is assumed to be ideally elastoplastic, as shown in Fig. 9*a*, with the yield strain, ε_{sy}, given by

$$[4] \quad \varepsilon_{sy} = \frac{f_y}{E_s}$$

The concrete stress–strain curves are also assumed to be elastoplastic, with the yield strain ε_{c1} and the ultimate strain ε_{cu}, as shown in Fig. 9*b*. The concrete modulus of elasticity, E_c (MPa), is equal to

$$[5] \quad E_c = 4700\sqrt{f'_c}$$

Forces acting on a radial segment

The forces on a radial segment (Fig. 10) can be summarized as follows: the external load or reaction, $P\Delta\Phi/2\pi$; tangential forces in the steel crossing the radial cracks and radial forces crossing the inclined crack, dF_{st} and dF_{sr}, respectively; forces in the concrete normal to the radial crack and forces in the concrete at the face of the column, dF_{cr} and dF_{ct}, respectively; and dowel forces in the steel crossing in the inclined crack, dD.

Steel forces

The idealized stress–strain curve for the reinforcing steel is shown in Fig. 9. For an orthogonal mesh type of reinforcement, with the bars equally spaced in both directions, the effec-

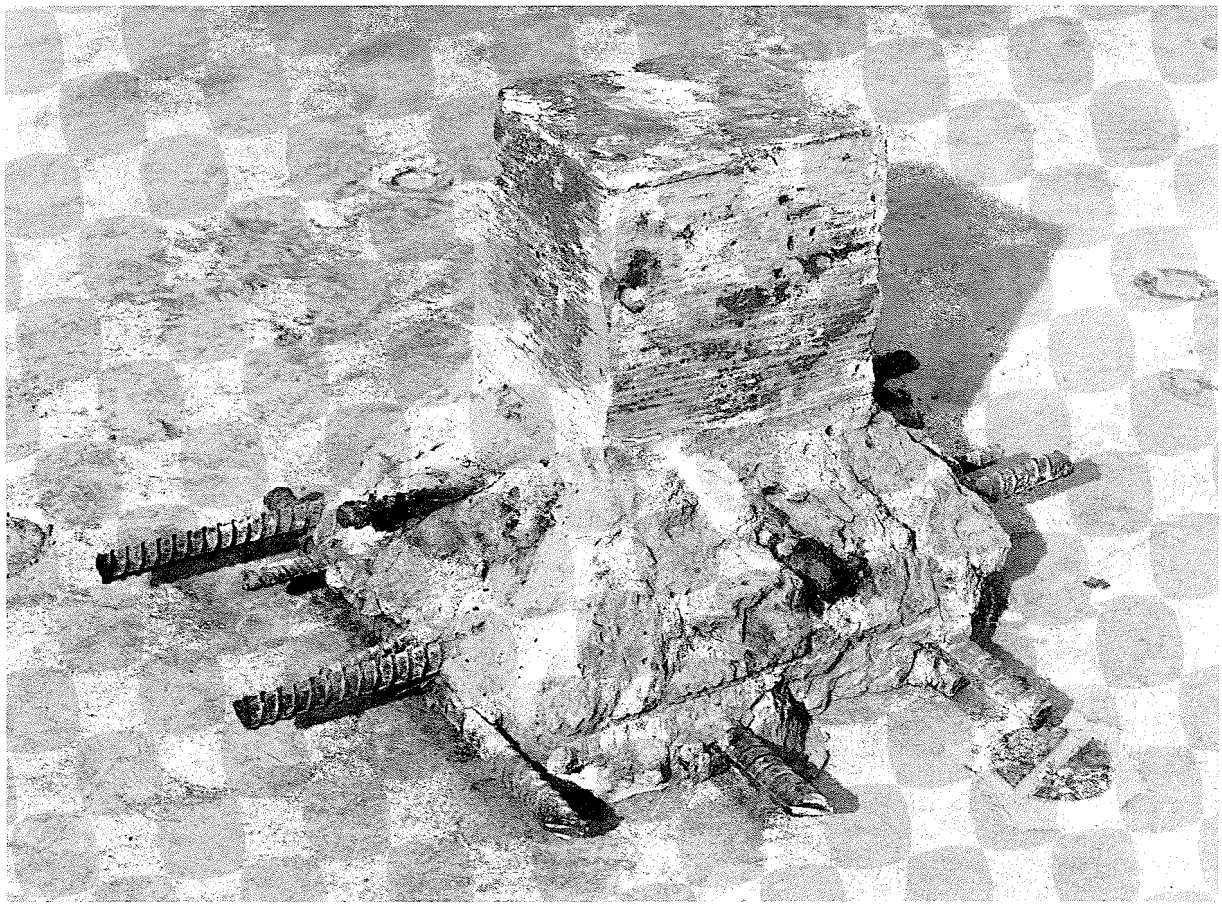

FIG. 5. Failure surface of a high-strength concrete slab.

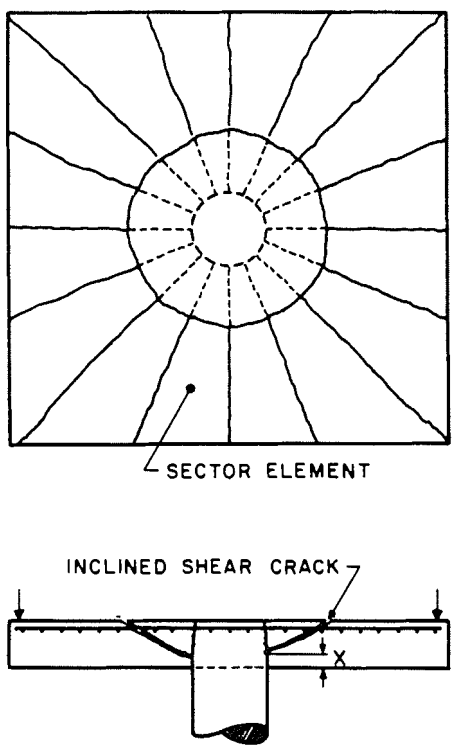

FIG. 6. Modified Kinnunen and Nylander punching model.

tive radial and tangential steel ratios are assumed equal. From the rigid-body rotation, the radius, r_y, within which all the flexural reinforcement yields is

$$[6] \quad r_y = \psi \frac{d}{\varepsilon_{sy}}\left(1 - \frac{x}{d}\right)$$

The total tangential steel force acting on a radial segment can be calculated using the following expressions:

If the radius of yield is smaller than the punching radius, i.e., $r_y < r_w$, then

$$[7] \quad F_{st} = \int_{r_w}^{r_3} \rho_t f_y d \, dr = \rho_t f_y d r_y \ln \frac{r_3}{r_w}$$

and if the radius of yield is greater than the punching radius, i.e., $r_y \geq r_w$, then

$$[8] \quad F_{st} = \int_{r_w}^{r_y} \rho_t f_y d \, dr + \int_{r_y}^{r_3} \rho_t f_y d \, dr = \rho_t f_y d[r_y - r_w] + r_y \ln \frac{r_3}{r_y}$$

Similarly, the radial forces in the flexural reinforcement acting on the radial segment are given by

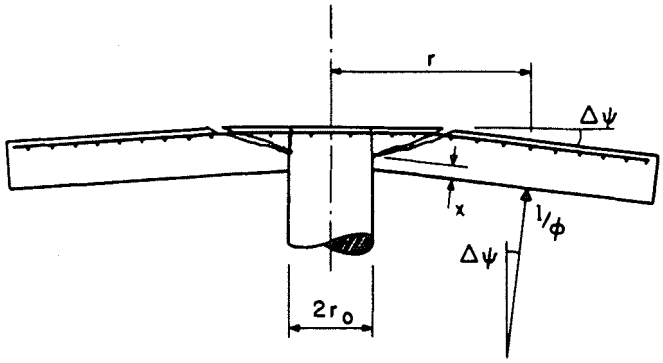

FIG. 7. Relation between deformation and strains.

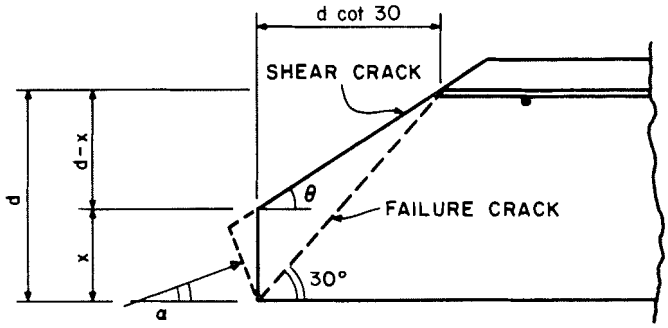

FIG. 8. Failure crack and assumed shear crack.

[9] $$dF_{sr} = \rho_r f_y dr_y \Delta\Phi, \qquad r_y < r_w$$

and

[10] $$dF_{sr} = \rho_r f_y dr_w \Delta\Phi, \qquad r_y \geq r_w$$

The total radial steel forces acting on the segment is equal to

[11] $$F_{stot} = dF_{sr} + F_{st}\Delta\Phi$$

Concrete forces

Each radial segment is supported by an inclined compressive force, as shown in Fig. 10. The magnitude of this force can be calculated from the maximum concrete bearing stress (Fig. 11), and hence the ultimate concrete forces at the column face, dF_{cr}, can be calculated from the following expression:

[12] $$dF_{cr} = \sigma_{bu} A_c$$

where A_c is the bearing area at the column head and σ_{bu} is the ultimate bearing strength of concrete given by

[13] $$\sigma_{bu} = \sqrt{\frac{r_0 + d}{r_0}}\, f'_c \leq 1.4 f'_c$$

The tangential concrete force acting on a radial element at radius r and thickness dr is

[14] $$F_{ct} = K_c f'_c x \, dr$$

where K_c is a function that defines the stress block according to the idealized stress–strain curve for concrete shown in Fig. 9,

$$K_c = \begin{cases} 0.425\varepsilon_c/\varepsilon_{c1}, & \varepsilon_c \leq \varepsilon_{c1} \\ 0.85(1 - \varepsilon_{c1}/2\varepsilon_c), & \varepsilon_c > \varepsilon_{c1} \end{cases}$$

Integrating [14] from $r = r_0$ to $r = r_3$ gives the value of the tangential forces acting on a radial segment,

[15] $$F_{ct} = \int_{r_0}^{r_{\varepsilon_c = \varepsilon_{c1}}} K_c f'_c x \, dr + \int_{r_{\varepsilon_c = \varepsilon_1}}^{r_3} K_c f'_c x \, dr$$

Dowel forces

The dowel forces are calculated from the equilibrium of the wedge element shown in Fig. 10,

[16] $$dD(r_w - r_0) = \rho_r d(\sigma_{s(r_w)} r_w - \sigma_{s(r_0)} r_0) + \left(\int_{r_0}^{r_w} \rho_r f_y d \, dr\right)\Delta\Phi$$

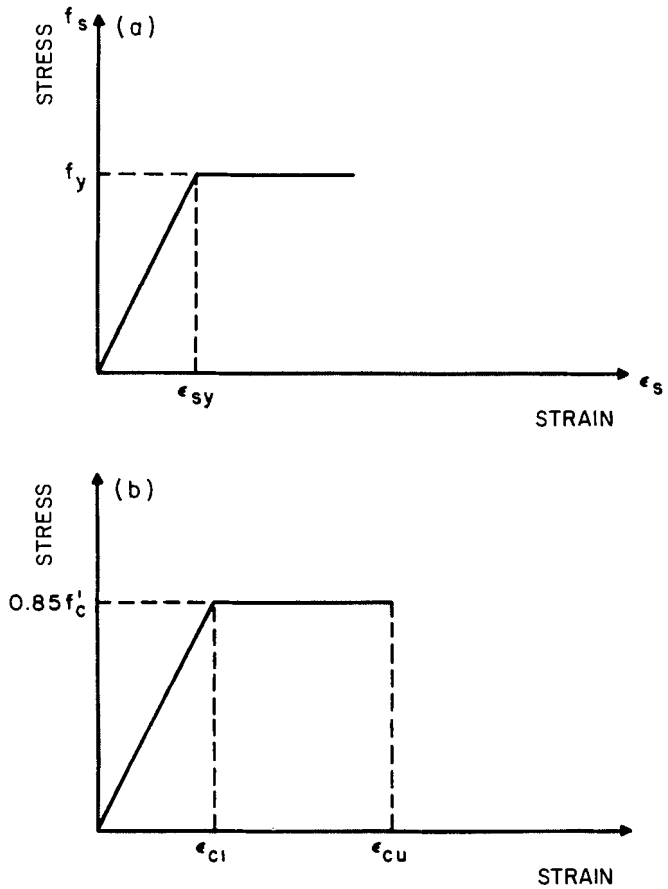

FIG. 9. Idealized stress–strain curves for (*a*) steel and (*b*) high-strength concrete.

Hence the dowel forces can be calculated using the following expressions:

[17] $$dD = \frac{d - x}{r_w - r_0} \rho_r f_y dr_y \ln\frac{r_w}{r_y} \Delta\Phi, \qquad r_y < r_w$$

and

[18] $$dD = 0, \qquad r_y \geq r_w$$

Calculation of the ultimate load

The three equilibrium equations of forces acting on a segment in a radial plane are as follows:

(*i*) The equilibrium of forces in a horizontal direction,

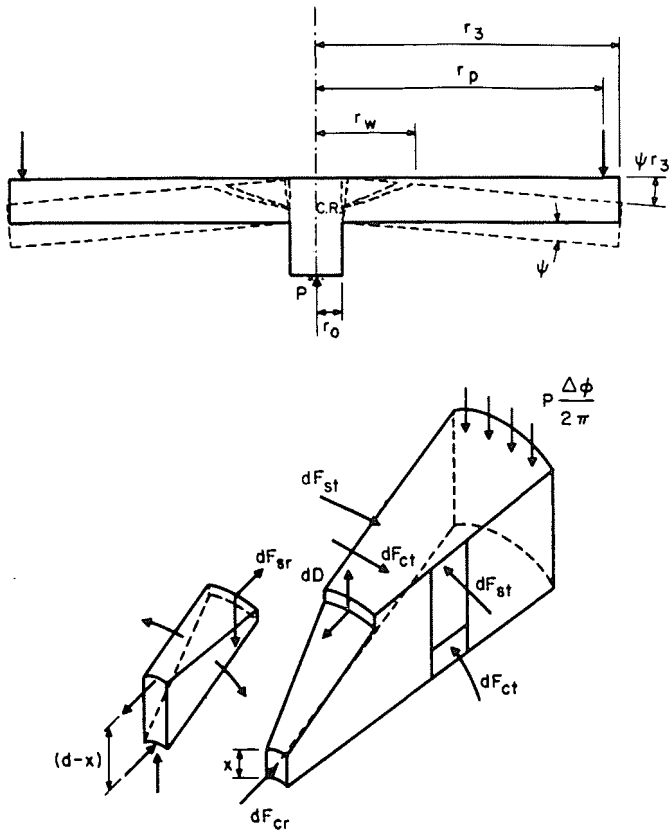

FIG. 10. Punching failure model and forces.

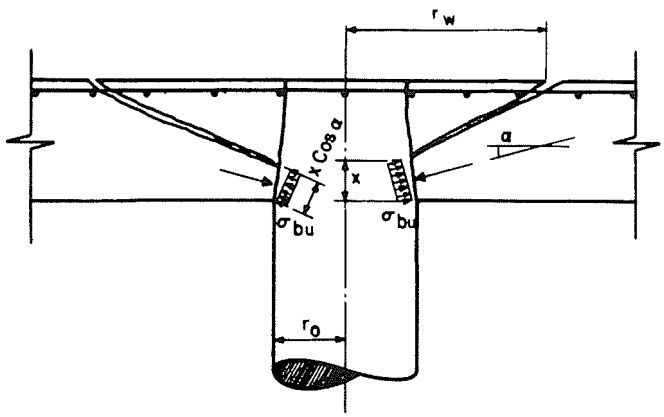

FIG. 11. Bearing stress failure at the column face.

[19] $dF_{cr} \cos \alpha + F_{ct} = dF_{sr} + F_{st}\Delta\Phi$

(*ii*) The equilibrium of vertical forces acting on a segment,

[20] $P\frac{\Delta\Phi}{2\pi} = dF_{cr} \sin \alpha + dD$

(*iii*) The moment with respect to the point of interaction of the resultant of F_{st} and the external load,

[21] $P\frac{\Delta\Phi}{2\pi}(r_p - r_0) = (dF_{sr} + dF_{st}\Delta\Phi)z + dD(r_w - r_0)$

where z is the lever arm.

By solving these three nonlinear equations, the inclination of the compressive forces at the column face, α, the neutral axis depth, x, and the punching load, P, can be determined. A computer program was developed to solve the three nonlinear simultaneous equations of equilibrium. The algorithm used was to calculate the values of α, x, and P for an assumed angle of rotation, ψ, and check for the occurrence of failure. If failure does not occur, then another value of ψ is assumed and the whole cycle is repeated until the failure criterion is satisfied. The values of α, x, and P at failure are then determined.

Failure criteria

Failure is assumed to occur when one of these criteria is satisfied:

1. if the yielding of tension reinforcement is reached in the whole slab;
2. if the tangential strain at the column periphery reaches a characteristic value of 0.0035;

[22] $\varepsilon_{ct} = \psi_f \frac{x}{r_0} \leq 0.0035$

Discussion

A comparison of the test results with the results of the proposed model is shown in Table 3. The proposed model provides better results, when compared with other models like Kinnunen and Nylander's model (1960) and Shehata and Regan's model (1989). The model was also used to predict the punching capacity of high-strength slabs (Hussein 1990), other slabs tested by Elstener and Hognestad (1956), Kinnunen and Nylander (1960), and Kinnunen *et al.* (1978).

The proposed model provides a more accurate prediction of the punching capacity of concrete slabs in general and high-strength concrete in particular. Although the proposed model utilizes some of Shehata and Regan's (1989) improvements of the original Kinnunen and Nylander's model by allowing the deformation of the portion of the slab that is on the top of the column and bounded by the shear crack, the proposed model does not recognize the stress gradient at the failure zone nor the lateral splitting of concrete as assumed by Shehata and Regan. Rather, it assumes that the bearing capacity reaches a limiting value at the column face.

The experimental evidence indicated that the failure is localized at the column face and does not occur over the whole front panel at the column face. Therefore, the restricted crushing nature of the concrete at the column face indicates a direct bearing failure. Test results also showed that the concrete strain measurements in the radial direction never reached the values recommended by Shehata and Regan's model (1989). Although the radial strains sometimes exceed the tangential strains at the column face, this occurs at locations very close to the column face and extends over a short distance. Near failure, the radial strains tend to decrease as observed experimentally.

The proposed model did not assume any limiting value of the angle of inclination of the compressive force at the column face, α, as recommended by other models. Nevertheless, the angle α must be established from the model equilibrium as explained earlier.

According to Shehata's (1985) finite element analysis, the limiting value of $\alpha = 20°$, in the authors' opinion, can only be true for elastic analysis only. However, near failure, the concrete adjacent to the column head is far from elastic. Therefore, the assumption of a limiting value of $\alpha = 20°$ is definitely not valid close to failure.

TABLE 3. Comparison of theoretical results with test results

Authors	Slab no.	d (mm)	c (mm)	r_3 (mm)	ρ (%)	f'_c* (MPa)	f_y (MPa)	$\frac{P_{calc}}{P_{test}}$†	$\frac{P_{calc}}{P_{test}}$‡	$\frac{P_{calc}}{P_{test}}$§	$\frac{P_{ACI}}{P_{test}}$	$\frac{P_{CEB}}{P_{test}}$
Marzouk and Hussein (high-strength concrete slabs)	NS1	95	150	1500	1.47	42	490	0.79	1.04	0.94	0.63	0.71
	HS1	95	150	1500	0.49	67	490	0.89	0.94	0.92	1.42	1.25
	HS2	95	150	1500	0.84	70	490	0.92	1.05	1.04	1.04	1.05
	HS7	95	150	1500	1.19	74	490	0.79	0.94	0.92	0.75	0.85
	HS3	95	150	1500	1.47	69	490	0.85	1.04	1.03	0.72	0.89
	HS4	90	150	1500	2.37	66	420	0.78	0.94	0.92	0.56	0.86
	NS2	120	150	1500	0.94	30	490	0.95	0.93	0.90	0.59	0.52
	HS5	125	150	1500	0.64	68	490	1.05	1.02	0.99	1.03	0.93
	HS6	120	150	1500	0.94	70	490	0.96	0.88	0.92	0.74	0.74
	HS8	120	150	1500	1.11	69	420	1.11	1.15	1.04	0.82	0.87
	HS9	120	150	1500	1.61	74	420	1.15	1.23	1.06	0.68	0.85
	HS10	120	150	1500	2.33	80	420	1.21	1.33	1.10	0.60	0.91
	HS11	70	150	1500	0.95	70	490	0.68	0.70	0.78	0.87	0.94
	HS12	70	150	1500	1.52	75	490	0.68	0.70	0.81	0.69	0.90
	HS13	70	150	1500	2.00	68	490	0.71	0.76	0.84	0.63	0.92
	HS14	95	220	1500	1.47	72	490	0.85	0.85	0.97	0.68	0.85
	HS15	95	300	1500	1.47	71	490	0.96	0.87	0.99	0.75	0.96
Elstner and Hognestad	A-1a	117	254	1780	1.15	14.1	332	1.05	0.90	0.96	0.72	0.61
	A-1b	117	254	1780	1.15	25.2	332	1.00	0.92	0.97	0.80	0.75
	A-1c	117	254	1780	1.15	29.0	332	1.06	0.98	1.01	0.88	0.85
	A-1d	117	254	1780	1.15	36.8	332	1.13	1.03	1.03	1.00	1.00
	A-1e	117	254	1780	1.15	20.2	332	0.98	0.89	0.94	0.73	0.67
	A-2a	114	254	1780	2.47	13.7	321	1.17	1.07	1.15	0.62	0.75
	A-2b	114	254	1780	2.47	19.5	321	1.10	1.05	1.11	0.62	0.79
	A-2c	114	254	1780	2.47	37.5	321	1.20	1.19	1.25	0.73	1.05
	A-7b	114	254	1780	2.47	28.0	321	0.98	0.96	1.03	0.58	0.79
	A-3a	114	254	1780	3.70	12.8	321	1.20	1.13	1.21	0.56	0.86
	A-3b	114	254	1780	3.70	22.6	321	1.18	1.23	1.19	0.60	1.00
	A-3c	114	254	1780	3.70	26.6	321	1.05	1.10	1.14	0.54	0.93
	A-3d	114	254	1780	3.70	34.6	321	1.14	1.20	1.24	0.60	1.09
	A-4	117	356	1780	1.15	26.2	321	1.13	0.94	0.94	0.94	0.91
	A-5	114	356	1780	2.47	27.8	321	1.27	1.07	1.22	0.70	0.98
	B-9	114	254	1780	2.00	43.9	341	1.09	1.06	1.11	0.73	0.97
	B-11	114	254	1780	3.00	13.5	408	1.25	1.25	1.23	0.62	0.85
	B-14	114	254	1780	3.00	50.5	325	1.17	1.20	1.14	0.69	1.16
Kinnunen and Nylander	5	117	ϕ150	ϕ1710	0.80	27.8	441	1.00	0.97	0.75	0.66	0.60
	6	118	ϕ150	ϕ1710	0.79	27.2	454	0.95	0.92	0.70	0.61	0.56
	24	128	ϕ300	ϕ1710	1.01	27.4	455	0.93	0.99	0.99	0.68	0.66
	25	124	ϕ300	ϕ1710	1.04	26.0	451	0.92	0.96	0.99	0.67	0.66
	32	123	ϕ300	ϕ1710	0.49	27.3	448	0.96	0.89	0.90	1.08	0.87
	33	125	ϕ300	ϕ1710	0.48	27.6	462	0.99	0.93	0.93	1.11	0.89
Kinnunen, Nylander and Tolf	b-1	100	ϕ125	ϕ1200	0.80	29.6	706	1.13	1.29	1.07	0.64	0.60
	b-3	99	ϕ125	ϕ1200	0.81	23.7	701	1.15	1.32	1.10	0.63	0.57
	b-5	200	ϕ250	ϕ2400	0.80	25.2	657	1.47	1.49	1.28	0.78	0.66
	b-6	199	ϕ250	ϕ2400	0.80	23.7	670	1.43	1.47	1.27	0.76	0.64
	b-13	98	ϕ125	ϕ1200	0.35	27.6	720	1.06	1.04	0.90	0.90	0.70
	b-14	99	ϕ125	ϕ1200	0.34	26.1	712	1.03	1.00	0.89	0.87	0.67
	b-17	200	ϕ250	ϕ2400	0.34	26.7	668	1.18	1.04	1.00	0.98	0.71
	b-18	197	ϕ250	ϕ2400	0.35	25.1	664	1.27	1.13	1.02	1.04	0.74

*$f'_c = 0.83 f_{cube}$.
†Kinnunen and Nylander (1960).
‡Shehata and Regan (1989).
§Proposed model.

Conclusions

A mechanical model was adopted and developed for the punching shear of high-strength concrete slabs. The model is based on experimental evidence and strain measurements for the tested slabs. The steel dowel forces, the angle of inclination of the concrete compressive forces at the column face, α, the angle of rotation, ψ, and the depth of the neutral axis, x, are calculated from the equilibrium equations. The forces in

the concrete slab in the tangential and radial directions are calculated using an appropriate idealization for the high-strength concrete. In the tangential direction, a limiting strain value is assumed at the column face, but never exceeds a limiting value of 0.0035. In the radial direction, the local bearing stress is assumed to take a limiting value at the column face. The proposed model provides good agreement between the predicted and experimental punching loads.

AMERICAN CONCRETE INSTITUTE. 1989. Building code requirements for reinforced concrete (ACI 318-89). American Concrete Institute, Detroit, MI.

BRITISH STANDARD INSTITUTION. 1985. Structural use of concrete, Part 1, Code of practice for design and construction (BS 8110:1985). British Standards Institution, London, United Kingdom.

CANADIAN STANDARDS ASSOCIATION. 1984. Design of concrete structures for buildings (CAN3-A23.3-M84). Canadian Standards Association, Rexdale, Ont.

CEB-FIP. 1987. Model for concrete structures. Comité Euro-International du Béton/Fédération Internationale de la Précontrainte, Paris, France.

ELSTENER, R. C., and HOGNESTAD, E. 1956. Shearing strength of reinforced concrete slabs. Journal of the American Concrete Institute, **53**(1): 29–58.

HUSSEIN, A. 1990. Behaviour of reinforced concrete slabs made with high-strength concrete. M.Eng. thesis, Memorial University of Newfoundland, St. John's, Nfld.

KINNUNEN, S., and NYLANDER, H. 1960. Punching of concrete slabs without shear reinforcement. Transactions No. 158, Royal Institute of Technology, Stockholm, Sweden.

KINNUNEN, S., NYLANDER, H., and TOLF, P. 1978. Investigations on punching at the Division of Building Statics and Structural Engineering, Nordisk Betong, No. 3, pp. 25–27.

MOE, J. 1961. Shearing strength of reinforced concrete slabs and footings under concentrated loads. Development Department Bulletin D47, Portland Cement Association, Skokie, IL.

REGAN, P. 1974. Design for punching shear. Proceedings, The Structural Engineer, London, United Kingdom, **52**(6): 197–207.

REGAN, P. E., and BRAESTRUP, M. W. 1985. Punching shear in reinforced concrete: a state-of-the-art report. Bulletin d'Information No. 168, Comité Euro-International du Béton, Lausanne, Switzerland.

SHEHATA, I. A. 1985. Theory of punching in concrete slabs. Ph.D. thesis, Polytechnic of Central London, London, United Kingdom.

SHEHATA, I. M., and REGAN, P. 1989. Punching in R.C. slabs. ASCE Journal of the Structural Division, **115**(ST7): 1726–1740.

List of symbols

c	side dimension of a square column
d	slab effective depth
dF_{cr}	radial concrete force
dF_{sr}	radial steel force
E_c	modulus of elasticity of concrete
E_s	modulus of elasticity of steel
F_{ct}	tangential concrete force
F_{st}	tangential steel force
F_{stot}	total steel forces in a radial direction
f'_c	compressive cylinder strength of concrete
f_y	yield strength of reinforcing steel
h	slab overall thickness
K	coefficient
P_{test}	ultimate test load
r_0	radius of column or loaded area
r_p	radius to the loading
r_w	radius of punch
r_y	radius within which all flexural reinforcement yield
r_3	radius of a slab
x	neutral axis depth
z	lever arm
α	angle of indication of the concrete force at the column face
ε_c	concrete strain
ε_{c1}	$0.85f'_c/4700\sqrt{f'_c}$
ε_{ct}	concrete tangential strain
ε_{cu}	concrete ultimate strain
ε_{st}	steel tangential strain
ε_{sy}	yield strain of reinforcing steel
ρ	reinforcement ratio (A_s/bd)
ρ_r	ratio of radial reinforcement
ρ_t	ratio of tangential reinforcement
$\Delta\Phi$	small sectorial angle of a radial segment
ψ	rotation of the slab portion outside the shear crack
ψ_f	rotation at failure
σ_{bu}	limiting bearing strength